International Journal of Heat and Mass Transfer 136 (2019) 1096–1105

Contents lists available at ScienceDirect

International Journal of Heat and Mass Transfer

journal homepage: www.elsevier.com/locate/ijhmt

Turbulent heat transfer optimization for solar air heater with variation method based on exergy destruction minimization principle

Hui Xiao, Junbo Wang, Zhichun Liu, Wei Liu *

School of Energy and Power Engineering, Huazhong University of Science and Technology, Wuhan 430074, PR China

ARTICLE INFO

Article history:
Received 14 May 2018
Received in revised form 9 March 2019
Accepted 12 March 2019

Keywords:
Heat transfer optimization
Solar air heater
Exergy destruction minimization
Longitudinal swirl flow

ABSTRACT

In this paper, a heat transfer optimization approach is brought in with focusing on exergy destruction to properly deal with the trade-off between irreversibility of heat transfer process and pump power consumption in turbulent flow for solar air heater. Thus, the exergy destruction minimization principle is mathematically extended to three dimensional turbulent flow and governing equations are derived with variation method. Successively, the optimized flow field for solar air heater is obtained at Re = 12,000 by applying SST k–ω turbulence model. Furthermore, with detail analysis of velocity and temperature distribution, it is found that the longitudinal swirl flow is generated through this optimization approach. Besides, within the scope of this study, the total heat transfer exergy destruction and average absorber temperature are maximally decreased by about 65% and 30 K respectively in the test section compared with the plain duct. And the maximum Nusselt number and friction factor are increased to 1.81 and 3.13 times over plain duct respectively. These results indicate that the optimization approach is effective for improving the thermal-hydraulic performance of solar air heater. Finally, the inclined vortex plate is designed to realize this kind of optimized flow field successfully. This work will promote technique developments of solar air heater.

1. Introduction

Solar energy, which is environmental friendly and abundant, is regarded as the linchpin of sustainable energy development program [1–3]. Solar air heaters are widely applied in many fields including space heating, crop drying, water desalination, textile etc. [1] due to their inherent simplicity, easy maintenance, and cost effectiveness. It is important to improve the thermal-hydraulic performance of solar air heater in turbulent flow owing to excessive heat loss to environment. In order to improve the thermal efficiency of solar air heater, many researchers concentrate on increasing heat transfer coefficient in the air side so as to decrease the absorber temperature, thereby reducing the heat loss to environment. Fins are applied to increase the efficiency of solar air heaters from the perspective of expanding heat transfer area [4–6]. Besides, artificial roughness on the absorber plate is effective to enhance forced convective heat transfer with moderate increase of friction factor in solar air heater ducts [7,8]. Bhushan and Singh [9] carried out an experimental investigation to analyze the effect of protruded roughness in a rectangular channel. Kumar et al. [10] experimentally studied the thermal performance of multi v-shaped rib with gap roughness on the heated plate, which showed that Nusselt number was enhanced much over smooth duct. Jin et al. [11] numerically investigated the effect of staggered multiple V-shaped ribs on thermo-hydraulic performance. Yadav and Bhagoria [12] presented a two-dimensional numerical investigation of the effect of equilateral triangular sectioned rib roughness on heat transfer and fluid flow in an artificially roughened solar air heater. Other heat transfer components, such as spherical inserts [13], baffles [14] and heat storage materials [15], also have drawn wide attention in recent years.

However, the design of a heat transfer component relies heavily on skills and experience of designers. The effectiveness is somewhat random with widely varied overall performance. Thus, it gives the author a hint that the design efficiency may be raised when heat transfer components are designed under the guidance of optimized flow field. Hence, it becomes a primary issue to find the optimized flow pattern for solar air heaters.

With variation method introduced into viscous flow problems [16], some researchers focused on applying the functional variation method to obtain optimized flow field [17–20], which is called heat transfer optimization. Wang et al. [21,22] optimized the convective heat transfer of laminar flow in the tube with the application of exergy destruction minimization, which significantly increased the heat transfer rate. In this study, the available potential is

* Corresponding author.
E-mail address: w_liu@hust.edu.cn (W. Liu).

https://doi.org/10.1016/j.ijheatmasstransfer.2019.03.071
0017-9310/

Nomenclature

A, B, C_0	Lagrange multipliers
C_p	specific heat capacity
D_h	hydraulic diameter
EEC	efficiency evaluation criterion
$E_{xd,\Delta T}$	total exergy destruction of heat transfer
$E_{xd,\Delta p}$	total exergy destruction of fluid flow
$e_{xd,\Delta T}$	local exergy destruction rate of heat transfer
$e_{xd,\Delta p}$	local exergy destruction rate of fluid flow
f	friction factor
H	duct height
h	heat transfer coefficient
I	turbulence intensity
J	Lagrange functional
k	turbulence kinetic energy
L	test section length
L_1	inlet section length
L_2	outlet section length
Nu	Nusselt number
P	pump power consumption
PEC	performance evaluation criterion
Pr	Prandtl number
Pr_t	turbulent Prandtl number
p	pressure
q	effective solar heat flux
Re	Reynolds number
S_g	entropy generation rate
T	time averaged temperature
T_0	ambient temperature
T_m	fluid bulk temperature
T_w	mean absorber wall temperature
$T_w(x)$	local averaged absorber wall temperature
U	time averaged velocity vector
u_r	maximum tangential velocity in the cross section
u_m	inlet mean velocity
V	volume
W	duct width
x,y,z	Cartesian coordinates

Greek symbol

β,θ	field synergy angles
κ	thermal conductivity
κ_t	turbulent thermal conductivity
κ_{eff}	effective thermal conductivity
μ	dynamic viscosity
μ_t	turbulent dynamic viscosity
μ_{eff}	effective dynamic viscosity
ρ	fluid density
Φ	viscous dissipation
Ω	control volume
ω	specific dissipation rate

introduced as a new thermodynamic parameter, which is defined as $e = h\text{-}T_0s$. In the meanwhile, Liu et al. [23–25] proposed some effective methods to realize the longitudinal swirling flow which was obtained through the above optimization. Recently, Liu et al. [26] optimized the catalyst porosity distribution in solar parabolic trough receiver-reactors by the variation method so that the solar energy was utilized more effectively. These previous results inspire the author to utilize variation method to find the optimized flow pattern.

In addition, exergy analyses can express the irreversibility of heat transfer process as well as evaluate the performance of solar energy system effectively based on the second law of thermodynamics [27–29]. Particularly, focusing on energy and exergy analyses, Alta et al. [4] conducted an experimental comparison study of three different solar air heater types, which presented that thermal efficiency increased with the decrease of irreversibility. In other words, heat transfer can be effectively enhanced by the way of minimizing exergy destruction. Lower heat transfer exergy destruction usually indicates lower temperature difference of the research object. Besides, a narrower temperature difference between working fluid and heat exchange surface means that the heat transfer coefficient has been improved. In this case, the heat transfer performance can be enhanced when heat transfer exergy destruction is reduced. Thus, heat transfer enhancement is consistent with exergy destruction minimization.

Therefore, it is a prospective study to obtain optimized flow field of solar air heater with exergy destruction minimization principle to guide the design of heat transfer components. In the following, the mathematics physics model of solar air heater is established firstly. And then, the exergy destruction minimization principle is extended to turbulent flow so that the optimized flow field can be obtained with applying SST k–ω turbulence model. Furthermore, the optimized results are displayed to elaborate fluid flow and heat transfer pattern with detail analyses of temperature contour, velocity distribution, absorber wall temperature, and exergy destruction. Finally, the novel inclined vortex plate is suggested for improving the thermal-hydraulic performance of solar air heater under the guidance of optimized flow field.

2. Computational physical model

2.1. Physical model and boundary condition.

As depicted in Fig. 1(a), conventional solar air heater consists of glass cover, absorber plate, back insulated cover and blower [7]. In order to reduce the complexity of heat transfer in such solar air heater, the simplified horizontal simulation model is displayed in Fig. 1(b). The total length is 1500 mm including inlet section, test section, and outlet section. The absorber plate is fixed at the top of the duct and the length of test section is 1000 mm. The inlet length and outlet length are 330 mm and 170 mm respectively, which follows the suggestion of ASHRAE standard 93-2003 for turbulent flow regime [30]. The height H is equal to 25 mm and the width W is 300 mm. Hence, the hydraulic diameter is 46.15 mm [31].

For saving computational resources, the width of computational domain is from $z = 0$ to $z = W/2$ and a symmetry boundary condition at the $z = 0$ plane is used. A uniform effective solar heat flux of 1000 W/m^2 is imposed on the absorber plate [10–12]. In the numerical simulation process, the temperature boundary condition at the top of inlet section is also a uniform heat flux of 1000 W/m^2 so as to guarantee no temperature entrance effects on the test section. Other walls are all adiabatic. The velocity and temperature are both uniform at the inlet of the duct and given as 4.15 m/s and 300 K, respectively. Thus, the Reynolds number is 12,000 and the turbulent intensity at the inlet can be estimated as [14]:

$$I = 0.16Re^{-1/8} \tag{1}$$

In addition, the pressure outlet boundary condition is specified at the outlet of the duct.

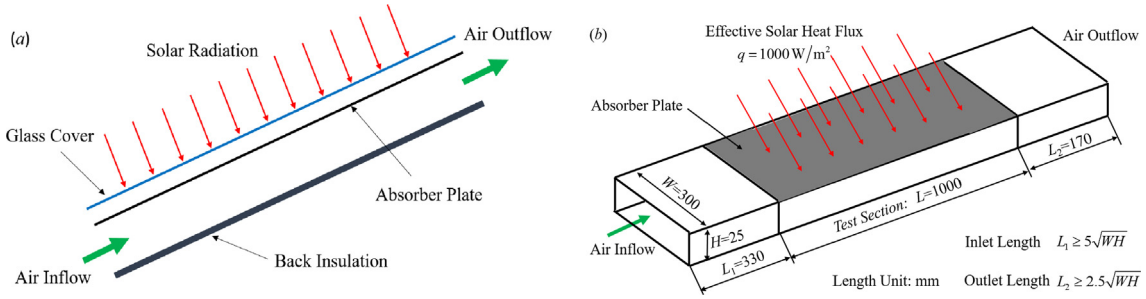

Fig. 1. Conventional solar air heater (*a*) and simplified simulation model (*b*).

2.2. Parameter definitions.

Thermophysical characteristics are important to heat transfer and fluid flow. The density (ρ) and specific heat (C_p) are assumed to be constant at 1.165 kg/m^3 and 1005 J/(kg·K) respectively. In order to reflect heat transfer and fluid flow characteristics more accurately, both laminar dynamic viscosity and thermal conductivity are varied with temperature. When the air temperature ranges from 280 K to 470 K, the following correlations are applied to estimate the laminar dynamic viscosity (μ) and thermal conductivity (κ) of air[6]:

$$\mu = \left(1.6157 + 0.06523T - 3.0297 \times 10^{-5}T^2\right) \times 10^{-6} \tag{2}$$

$$\kappa = \left(0.0015215 + 0.097459T - 3.3322 \times 10^{-5}T^2\right) \times 10^{-3} \tag{3}$$

In order to express the thermo-hydraulic characteristics in the duct, some related parameters which are Reynolds number (Re), friction factor (f), heat transfer coefficient (h), and Nusselt number (Nu) should be defined. Moreover, some parameters to evaluate the thermal-hydraulic performance should be also utilized. The related parameters are given as follows:

Reynolds number:

$$Re = \frac{\rho u_{\mathrm{m}} D_{\mathrm{h}}}{\mu} \tag{4}$$

Friction factor:

$$f = \frac{\Delta p}{(L/D_{\mathrm{h}})\rho u_{\mathrm{m}}^2/2} \tag{5}$$

Heat transfer coefficient:

$$h = \frac{q}{T_{\mathrm{w}} - T_{\mathrm{m}}} \tag{6}$$

Nusselt number:

$$Nu = \frac{hD_{\mathrm{h}}}{\kappa} \tag{7}$$

where u_{m} is the inlet mean velocity in the duct, T_{w} is the mean absorber plate wall temperature, and T_{m} is the fluid bulk temperature of test section in the rectangular duct.

Field synergy principle [32–34] is widespread in evaluating performance of convective heat transfer. Local field synergy angles β and θ, which represent heat transfer performance and flow resistance respectively, are defined as:

$$\beta = \arccos\frac{\boldsymbol{U}\cdot\nabla T}{|\boldsymbol{U}|\cdot|\nabla T|}, \quad \theta = \arccos\frac{\boldsymbol{U}\cdot(-\nabla p)}{|\boldsymbol{U}|\cdot|-\nabla p|} \tag{8}$$

Besides, integrated mean synergy angles in this paper are given as:

$$\beta_{\mathrm{m}} = \arccos\frac{\sum(\boldsymbol{U}\cdot\nabla T)_i dV_i}{\sum(|\boldsymbol{U}|\cdot|\nabla T|)_i dV_i}, \quad \theta_{\mathrm{m}} = \arccos\frac{\sum(\boldsymbol{U}\cdot(-\nabla p))_i dV_i}{\sum(|\boldsymbol{U}|\cdot|-\nabla p|)_i dV_i} \tag{9}$$

The performance evaluation criterion (PEC) proposed by Webb [35] is extensively used for heat transfer enhancement in exchanger design at identical pump power, which is calculated as:

$$\mathrm{PEC} = \frac{Nu/Nu_0}{(f/f_0)^{1/3}} \tag{10}$$

Another efficiency evaluation criteria (EEC) is written as the following form [22]:

$$\mathrm{EEC} = \frac{Nu/Nu_0}{f/f_0} \tag{11}$$

where Nu_0 and f_0 are empirical values of plain duct at the same Reynolds number, respectively.

As known from the formula expressions of the two evaluation criterion, EEC is more sensitive to resistance than PEC. Therefore, PEC is adopted to investigate the overall thermal-hydraulic performance while EEC is suitable for investigating the resistance reduction performance.

3. Exergy destruction minimization principle in turbulent flow

In order to describe the turbulent flow in solar air heater, the Reynolds-averaged Navier–Stokes equations are employed based on the Reynolds Stress Model. Besides, the velocity, temperature, and pressure are time averaged terms in this paper for convenience. For the purpose of simplifying the present three-dimensional, turbulent, and steady air flow, the following assumptions are adopted for the governing equations: (a) the fluid is continuous and incompressible, (b) the effects of gravity and volume dilation are negligible, and (c) natural convection and radiation are also not taken into consideration. Thus, the theoretical derivation of convective heat transfer optimization can be carried out in the following.

As for convective heat transfer problem without inner heat source, ignoring viscous dissipation in heat transfer process, the entropy generation rate can be written as [36]:

$$S_{\mathrm{g}} = \frac{\kappa_{\mathrm{eff}}(\nabla T)^2}{T^2} \tag{12}$$

where κ_{eff} is effective thermal conductivity in turbulent flow.

Thus, the total exergy destruction of heat transfer can be expressed as:

$$E_{xd,\Delta T} = \iiint_{\Omega} T_0 S_{\mathrm{g}} dV = \iiint_{\Omega} T_0 \frac{\kappa_{\mathrm{eff}}(\nabla T)^2}{T^2} dV \tag{13}$$

where the ambient temperature T_0 is equal to 298 K.

On the other hand, the total pump power consumption is equivalent to the sum of change in kinetic energy and viscous dissipation [37], which can be given as:

$$P = \iiint_{\Omega} [\rho \boldsymbol{U} \cdot (\boldsymbol{U} \cdot \nabla)\boldsymbol{U} + \Phi] dV \tag{14}$$

where the viscous dissipation Φ is given as:

$$\Phi = \frac{\mu_{\text{eff}}}{2}\left(\nabla \boldsymbol{U} + \nabla \boldsymbol{U}^{\mathrm{T}}\right)^2 \tag{15}$$

where μ_{eff} is effective dynamic viscosity in turbulent flow.

In the present problem, the pump power consumption is also equal to the total exergy destruction caused by pressure difference [22]. It can be given as:

$$\begin{aligned} P &= \iiint_{\Omega} [\rho \boldsymbol{U} \cdot (\boldsymbol{U} \cdot \nabla)\boldsymbol{U} + \Phi] dV = \iiint_{\Omega} \left(\nabla \cdot \left(\boldsymbol{U} \cdot \mu_{\text{eff}}\left(\nabla \boldsymbol{U} + \nabla \boldsymbol{U}^{\mathrm{T}}\right)\right) - \boldsymbol{U} \cdot \nabla p\right) dV \\ &= \iiint_{\Omega} (-\boldsymbol{U} \cdot \nabla p) dV = \iiint_{\Omega} e_{xd,\Delta p} dV \end{aligned} \tag{16}$$

The purpose of the present work is to deal with the trade-off between the irreversibility of heat transfer and power consumption in solar air heater. The optimized flow field can be obtained when the total exergy destruction of heat transfer is minimum with constant power consumption. Hence, with the constraint of continuity and energy equations, the Lagrange function of exergy destruction can be constructed as:

$$\mathrm{J} = \iiint_{\Omega} \left\{ \begin{array}{l} T_0 \frac{\kappa_{\text{eff}} (\nabla T)^2}{T^2} + \mathrm{C}_0 [\rho \boldsymbol{U} \cdot (\boldsymbol{U} \cdot \nabla)\boldsymbol{U} + \Phi] + \\ \mathrm{A} \nabla \cdot (\rho \boldsymbol{U}) + \mathrm{B}\left[\nabla \cdot (\kappa_{\text{eff}} \nabla T) - \rho C_p \boldsymbol{U} \cdot \nabla T\right] \end{array} \right\} dV \tag{17}$$

where A, B, and C_0 are Lagrange multipliers. A and B are functions of space, and C_0 is constant.

In order to get the optimized results, the variation calculus is taken on the above Lagrange function. With proper treatment to operator A and boundary condition [21], the variation of functional J can be simplified as:

$$\begin{aligned} \delta \mathrm{J} = & \iiint_{\Omega} \mathrm{C}_0 \left((\boldsymbol{U} \cdot \nabla)(\rho \boldsymbol{U}) - \nabla \cdot \left(\mu_{\text{eff}}\left(\nabla \boldsymbol{U} + \nabla \boldsymbol{U}^{\mathrm{T}}\right)\right) - \mathrm{B}\rho \tfrac{C_p}{\mathrm{C}_0} \nabla T + \nabla p\right) \delta \boldsymbol{U} dV \\ & + \iiint_{\Omega} \nabla \cdot (\rho \boldsymbol{U}) \delta \mathrm{A} dV + \iiint_{\Omega} \left(\nabla \cdot (\kappa_{\text{eff}} \nabla T) - \rho C_p \boldsymbol{U} \cdot \nabla T\right) \delta \mathrm{B} dV \\ & + \iiint_{\Omega} \left(\nabla \cdot (\kappa_{\text{eff}} \nabla \mathrm{B}) + \rho C_p \boldsymbol{U} \cdot \nabla \mathrm{B} + \frac{2T_0}{T^2}\left(\frac{\kappa_{\text{eff}}}{T} (\nabla T)^2 - \nabla \cdot (\kappa_{\text{eff}} \nabla T)\right)\right) \delta T dV \\ & + \oint_{\Gamma} \left[\left(2T_0 \tfrac{\kappa_{\text{eff}} \nabla T}{T^2} - \kappa_{\text{eff}} \nabla \mathrm{B}\right) \delta T + \mathrm{B} \delta (\kappa_{\text{eff}} \nabla T)\right] d\boldsymbol{S} \end{aligned} \tag{18}$$

Taking functional variation with respect to Lagrange multipliers A, B, **U**, and T on functional J, respectively, the governing equations for the optimized flow field can be obtained one by one. Thus, the optimized turbulent time-averaged partial differential equations can be constructed as:

Continuity equation:

$$\nabla \cdot (\rho \boldsymbol{U}) = 0 \tag{19}$$

Energy equation:

$$\rho C_p \boldsymbol{U} \cdot \nabla T = \nabla \cdot (\kappa_{\text{eff}} \nabla T) \tag{20}$$

Momentum equation:

$$\rho \boldsymbol{U} \cdot \nabla \boldsymbol{U} = -\nabla p + \nabla \cdot \left(\mu_{\text{eff}}\left(\nabla \boldsymbol{U} + \nabla \boldsymbol{U}^{\mathrm{T}}\right)\right) + \frac{C_p}{\mathrm{C}_0} \rho \mathrm{B} \nabla T \tag{21}$$

Scalar equation B:

$$-\rho \boldsymbol{U} \cdot \nabla \mathrm{B} = \nabla \cdot \left(\frac{\kappa_{\text{eff}}}{C_p} \nabla \mathrm{B}\right) + \frac{2T_0}{C_p T^2}\left(\frac{\kappa_{\text{eff}}}{T} (\nabla T)^2 - \nabla \cdot (\kappa_{\text{eff}} \nabla T)\right) \tag{22}$$

where the boundary condition of Eq. (22) depends on the temperature boundary condition. The relationship can be expressed as:

$$\left(2T_0 \frac{\kappa_{\text{eff}} \nabla T}{T^2} - \kappa_{\text{eff}} \nabla \mathrm{B}\right) \delta T + \mathrm{B} \delta (\kappa_{\text{eff}} \nabla T) = 0 \tag{23}$$

When the temperature boundary condition is a constant heat temperature, it can be specified as:

$$\mathrm{B} = 0 \tag{24}$$

And when the temperature boundary condition is a constant heat flux, it can be specified as:

$$\nabla \mathrm{B} = \frac{2T_0 \nabla T}{T^2} \tag{25}$$

The source term $\rho C_p \mathrm{B} \nabla T / \mathrm{C}_0$ in Eq. (21), which is governed by energy equation and scalar equation B, represents the additional thermal effect exerted on fluid. In practice, as long as the real additional force which is equal to this source term is realized in momentum equation, the optimal fluid flow can be formed. As for numerical simulation, when the effective turbulent viscosity and thermal conductivity are calculated with proper turbulent model, the optimized flow field can be obtained by simultaneous solving Eqs. (19)–(22). For handling the coupling of pressure and velocity, there are some algorithms and the SIMPLE algorithm is usually selected [38,39]. Besides, the effective viscosity and thermal conductivity can be given as:

$$\mu_{\text{eff}} = \mu + \mu_{\mathrm{t}} \tag{26}$$

$$\kappa_{\text{eff}} = \kappa + \kappa_{\mathrm{t}} = \kappa + \mu_{\mathrm{t}} / Pr_{\mathrm{t}} \tag{27}$$

where μ_{t} and κ_{t} are turbulent viscosity and thermal conductivity, respectively. The turbulent Prandtl number Pr_{t} is usually equal to 0.85.

4. Computational model verification

The overall computational fluid dynamics (CFD) simulation is based on the commercial software FLUENT 16.0. Some methods are applied for the numerical simulation of heat transfer and turbulent fluid flow. The user defined function (UDF) and user defined scalar (UDS) are utilized so that the source term in Eq. (21) is included and that Eq. (22) can be solved. Some researchers have observed that the Shear Stress Transport (SST) k–ω turbulence model could provide good numerical results in three dimensional duct [13,40,41]. Thus, the SST k–ω turbulence model [42] is employed to deal with turbulence flow, which is expressed as:

$$\frac{\partial}{\partial t}(\rho k) + \frac{\partial}{\partial x_i}(\rho k u_i) = \frac{\partial}{\partial x_j}\left(\Gamma_k \frac{\partial k}{\partial x_j}\right) + G_k - Y_k \tag{28}$$

$$\frac{\partial}{\partial t}(\rho \omega) + \frac{\partial}{\partial x_i}(\rho \omega u_i) = \frac{\partial}{\partial x_j}\left(\Gamma_\omega \frac{\partial \omega}{\partial x_j}\right) + G_\omega - Y_\omega \tag{29}$$

where G_k represents the production of turbulence kinetic energy k; G_ω represents the generation of specific dissipation rate ω; Γ_k and Γ_ω represent the effective diffusivity of k and ω, respectively; Y_k and Y_ω represent the dissipation of k and ω due to turbulence. The low-Re correction is taken into consideration while curvature correction and production limiter are also applied. Besides, the turbulent viscosity can be calculated by utilizing k and ω, which is detailedly defined in Ref. [42]. In addition, the finite volume

formulation is applied to discretize the governing conservation equations with second order discretization scheme for pressure, second order upwind discretization scheme for energy, momentum, k, ω, and B. The SIMPLE algorithm is used to solve the puzzle of pressure-velocity coupling. When the relative energy residual value is less than 10^{-6} as well as others are less than 10^{-4} or all relative residual values keep constant, the calculation is considered to converge at the right results.

The hexahedral grids of the duct domain are generated with the software GAMBIT 2.4.6. For the sake of describing the complex flow in the boundary layer region, the enhanced wall treatment is employed and the meshes attached to the duct wall are extremely dense, which guarantees $y^+ \leqslant 1$. The grid independence has been carried out for the enhanced duct with optimized flow field when C_0 is equal to 5×10^3 and the Reynolds number is equal to 12,000. Model 1, Model 2, Model 3, and Model 4 represent four different grid numbers: 1.27 million, 2.67 million, 4.53 million, and 8.34 million, respectively. As the results displayed in Fig. 2, the computational deviation caused by mesh density is quite small when the grid number is greater than 4.53 million. The relative Nusselt number deviation and friction factor deviation between Model 3 and Model 4 is approximately −0.17% and −0.60%, respectively. Hence, the grid system of Model 3 is independent. The comparison of thermal–hydraulic characteristics between plain duct and empirical formula is also implemented to validate the numerical results of Model 3 at Re = 12,000. The empirical formulas of Nusselt number and friction factor are Dittus-Boelter correlation and Modified Blasius correlation [9–11].

Dittus-Boelter correlation:

$$Nu_0 = 0.023 Re^{0.8} Pr^{0.4} \tag{30}$$

Modified Blasius correlation:

$$f_0 = 4 \times 0.085 Re^{-0.25} \tag{31}$$

Compared with empirical formulas, errors of Nusselt number and friction factor are both less than 3%, which demonstrates that the grid system Model 3 is adequately accurate. Therefore, considering the compromise of solution precision and time consumption, the grid system of Model 3 is adopted in the following simulation.

5. Heat transfer optimization results discussion

In order to describe the optimized flow, the basic characteristics of flow and heat transfer pattern will be researched based on qualitative analyses, including temperature contours and velocity distributions in the cross section. Furthermore, the quantitative study of the optimized flow pattern will be carried out with analyses of exergy destruction, field synergy, Nu/Nu_0, f/f_0, and absorber wall temperature.

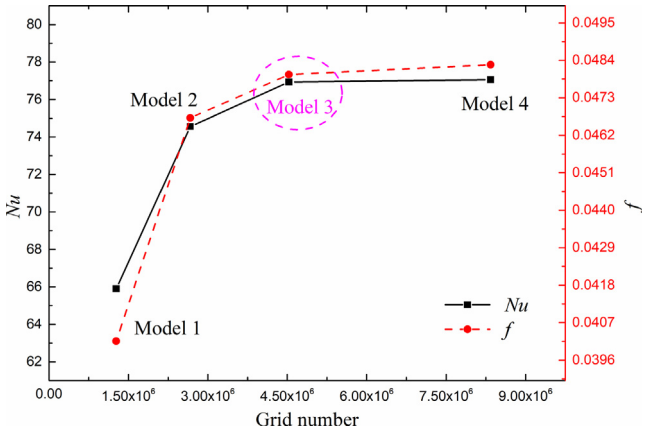

Fig. 2. Grid independence verification at Re = 12,000.

5.1. Heat transfer and fluid flow pattern

It shows in Fig. 3 four temperature contours in the cross section $\times$ = 0.8 m perpendicular to the x axis with different C_0 at Re = 12,000. The wall temperature is high in some places and low in other places at an arbitrary given C_0. The lower temperature of the fluid near the wall indicates an increased heat transfer coefficient. It is apparent that the temperature distribution is changed significantly with the decrease of C_0, because the additional thermal effect on flow field is stronger and stronger. With the disturbance on temperature field gradually enhanced, the change of temperature distribution appears in the boundary flow region first and then the mixing of hot and cold fluid is gradually thorough. As displayed in Fig. 3, the high temperature fluid tends to migrate from the absorber plate towards the bottom and the blue cold fluid is on the contrary. In addition, with the decrease of C_0, the range of temperature in the transverse section becomes narrower and narrower accompanied by a reduction of the temperature difference from 78 K to 38 K in the scope of research. It indicates that the temperature is distributed more uniform as a result of less exergy destruction caused by heat transfer. In this way, heat transfer is enhanced and the optimized temperature distribution is obtained in the view of exergy destruction minimization. In order to reveal the detail cause of such temperature distributions, the velocity distribution is discussed in the following.

As depicted in Fig. 4, it shows the variation of tangential velocity with different C_0 in the cross section of x = 0.8 m at Re = 12,000. It is observed that vortices are produced in the cross section, which indicates that longitudinal swirls are generated along the flow direction. These counter-rotating vortices bring cold fluid from the core region to scour the boundary layer and extrude the hot fluid in this area. In this way, the core flow rapidly reaches the boundary region, resulting in a lower temperature near the wall. Besides, with flowing along the duct, the fluid is sufficiently mixed so that the temperature tends to be uniform. Obviously, with the decrease of operator C_0, the influence scope of vortices becomes wider. For the decrease of C_0 causes the increase of additional thermal effect imposed on fluid, consequently the longitudinal swirl flow is enhanced to form large vortices. With the appearance of large vortices as well as the annihilation of some small vortices, the number of existing vortices tend to be decreased. On the other hand, with C_0 decreasing, small disturbance emerges prominently near the absorber wall. It is conducive to heat transfer and may lead to the generation of new small vortices. In addition, it can be found that the velocity ratio of maximum tangential velocity to mean velocity (u_r/u_m) is also increased in the cross section. The tangential velocity mixes hot and cold fluids and decreases the angle between velocity and temperature gradient, thus the convective heat transfer can be enhanced. However, due to the increase of tangential velocity, more related viscous dissipation is produced during fluid flow, leading to an increased pump power consumption. Further observation, it can be obtained, with the increase of pump power consumption, vortices are appeared in the boundary region first and then extended to core flow region. When vortices are strong enough in core region, new disturbance looms in the boundary region again. It indicates that the key region where extra heat transfer enhancement measures are urgently needed is varied from boundary flow region to core flow region and then back to boundary flow region, which depends on the increase of pump power consumption. With the application of heat transfer optimization, the pump power consumption can be effectively utilized in the key region of heat transfer enhancement.

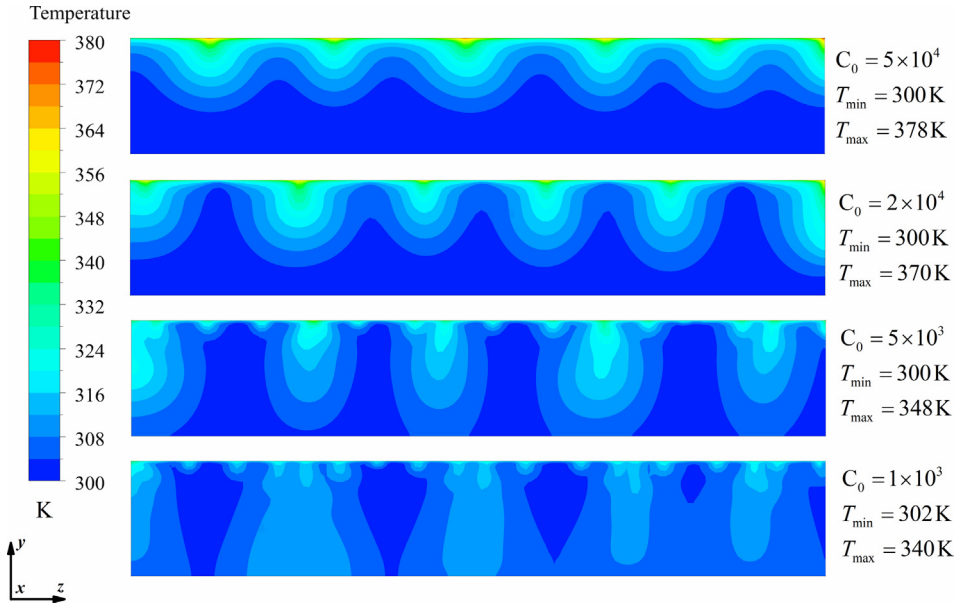

Fig. 3. Temperature contours with the variation of C_0 in the plane of x = 0.8 m.

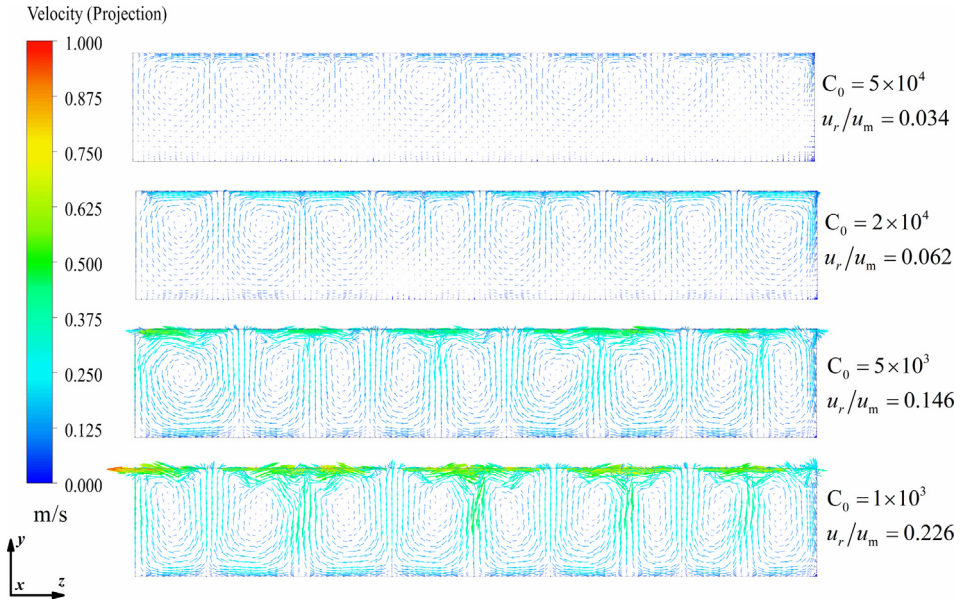

Fig. 4. Tangential velocity distribution with the variation of C_0 in the plane of x = 0.8 m.

Thus, the optimized flow field can achieve high heat transfer coefficient at low pump power consumption.

Therefore, temperature distribution and velocity distribution are closely related and the formation of temperature field can be attributed to the longitudinal swirling flow which is conducive to enhancing the overall thermal-hydraulic performance.

5.2. Exergy destruction analyses

The exergy destruction is the focus of this article so that the variation of exergy destruction should be displayed. Usually, the exergy destruction of heat transfer process is far larger than that of pump power consumption. That is to say, the exergy destruction needs to be divided into heat transfer exergy destruction and pump power consumption. And the two parts should be discussed separately. The expression of exergy destruction rate, which is equal to available potential loss, can be written in incompressible turbulent flow as [22]:

$$e_{xd} = e_{xd,\Delta T} + e_{xd,\Delta p} \tag{32}$$

where $e_{xd,\Delta T} = T_0 S_g$ and $e_{xd,\Delta p} = -\boldsymbol{U} \cdot \nabla p$.

Thus, the local integrated exergy destruction is defined as:

$$E_{xd}(x) = \int_{0.33}^{x} \int_{0}^{H} \int_{-W/2}^{W/2} e_{xd}(x,y,z) dz dy dx \tag{33}$$

It is shown in Fig. 5 local exergy destruction rate distributions caused by heat transfer ($e_{xd,\Delta T}$) and fluid flow ($e_{xd,\Delta p}$) in the plane of$x$ = 0.8 m with $C_0 = 5 \times 10^3$. Local heat transfer exergy destruction distribution rate is related to the corresponding temperature contour. Higher temperature gradient may result in higher heat transfer exergy destruction. Lower heat transfer exergy destruction

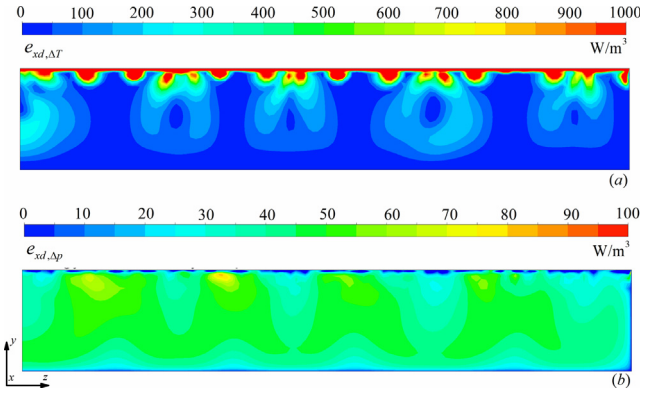

Fig. 5. Distributions of local exergy destruction rate caused by (*a*) temperature difference and (*b*) pressure loss in the plane of $x = 0.8$ *m*.

always indicates lower temperature difference. As is depicted in Fig. 5(a), it can be found that high heat transfer exergy destruction rate region is restricted to the area near the absorber wall, and that most region of the cross section accompanies with low heat transfer exergy destruction rate. In this way, total heat transfer exergy destruction has been minimized at a given power consumption with the variation method, leading to lower temperature difference of the whole domain. Thus, heat transfer performance has been improved. Comparing Fig. 5(a) with Fig. 5(b), it is found that low heat transfer exergy destruction rate is attributed to high exergy destruction rate of fluid flow. It is illustrated in Fig. 6 the local integrated exergy destruction along *x* direction. $E_{xd,\Delta T}(x)$ and $E_{xd,\Delta p}(x)$ are respectively caused by temperature difference and pressure difference of test section. Based on the optimization principle in this paper, the line in Fig. 6(a) is the lowest limit of local integrated exergy destruction of heat transfer process at the corresponding given pump power consumption presented in Fig. 6(b). Along with the increase of pump power consumption, the lowest limit is subsequently lower. The total heat transfer exergy destruction can be maximally reduced by about 65% compared with plain duct in the scope of research, which demonstrates the effectiveness of this optimization approach.

5.3. Thermal and hydraulic analyses

When C_0 ranges from 5×10^4 to 10^3, pump power consumption increases from 0.24 W to 0.4 W. As illustrated in Fig. 7, total heat transfer exergy destruction decreases as heat transfer performance is enhanced. As the heat transfer exergy destruction decreases, the mean synergy angle β_m also decreases, which means that the synergistic effect between velocity and temperature gradient is improved. Besides, both total exergy destruction of fluid flow and mean field synergy angle θ_m are increased with the increase of power consumption. In order to describe the characteristics of heat transfer and fluid flow intuitively, ratios Nu/Nu_0 and f/f_0 are utilized. On the whole, the maximum Nusselt number and friction factor are increased to 1.81 and 3.13 times over plain duct respectively within the scope of this study. It is clear that both Nu/Nu_0 and f/f_0 increase as pump power consumption increases. Due to the fact that the increase of Nu/Nu_0 exceeds that of f/f_0 with the increase of power consumption, the optimized flow field can achieve high heat transfer enhancement with low increase of resistance.

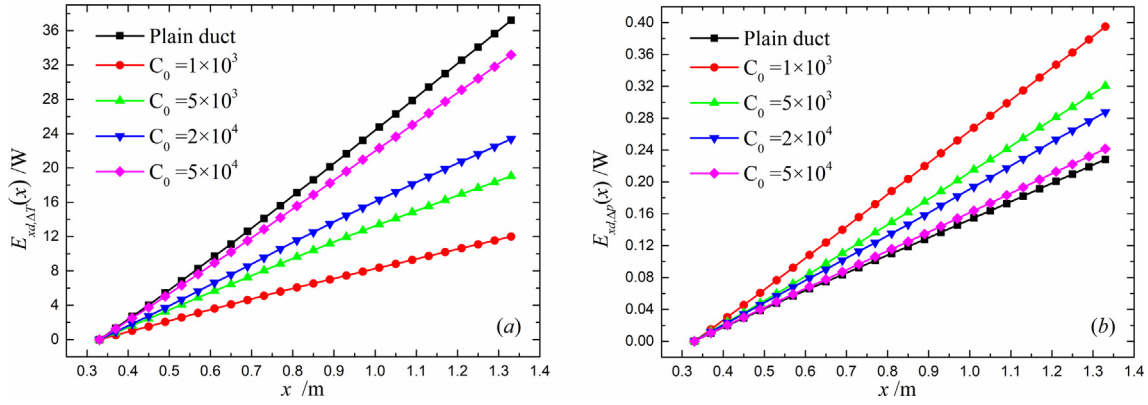

Fig. 6. The local integrated exergy destruction caused by (*a*) temperature difference and (*b*) pressure difference of test section along *x* direction.

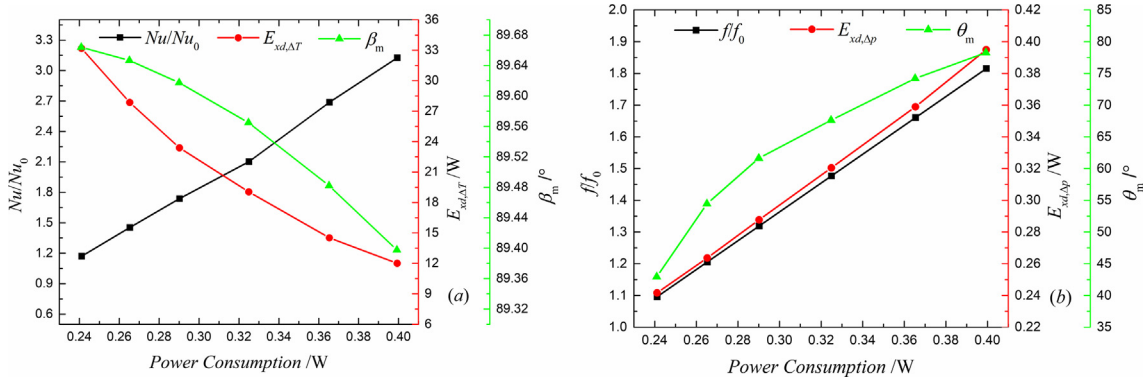

Fig. 7. Variations of thermal-hydraulic characteristics, total exergy destruction, and field synergy angles with the increase of power consumption.

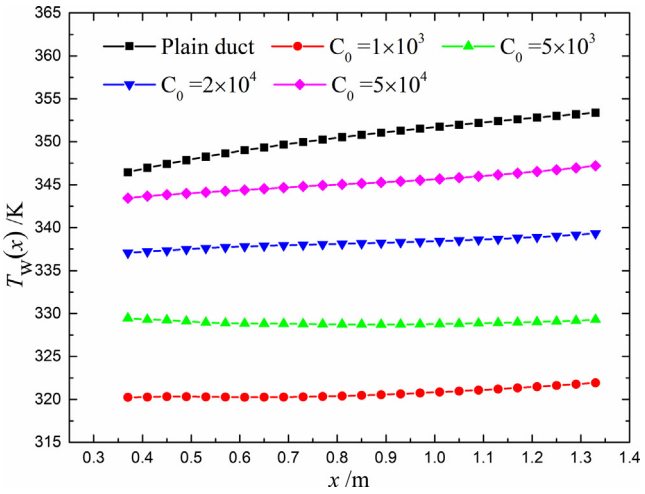

Fig. 8. Variations of local averaged absorber wall temperature of test section.

Absorber wall temperature is another important parameter for evaluating the heat transfer performance. Reducing absorber wall temperature can bring benefits of less heat loss to environment. A lower wall temperature indicates a better efficiency. The definition of local averaged absorber wall temperature is expressed as:

$$T_w(x) = \frac{\int_{0.33}^{x}\int_{-W/2}^{W/2} T(x,z)dzdx}{\int_{0.33}^{x}\int_{-W/2}^{W/2} dzdx} \tag{34}$$

As depicted in Fig. 8, the absorber wall temperature is decreased when C_0 is decreased. And the averaged absorber temperature can be maximally decreased by about 30 K compared with plain duct. When the longitudinal swirl is generated, the synergistic effect of velocity and temperature gradient is greatly improved due to the generation of tangential velocity. Besides, working fluid is mixed fully. In this case, heat transfer performance is enhanced so that the temperature difference reduces. Thus, heat transfer exergy destruction is decreased and the absorber wall temperature is lowered. In conclusion, the longitudinal swirl flow is an effective flow pattern for heat transfer enhancement.

6. Optimized flow pattern realization in solar air heater.

This part aims at the realization of optimized velocity field in solar air heater. The longitudinal swirl flow has been realized in tube through many methods, such as ribbed tube [24], slant rods inserts [23], and conical strips inserts [25]. Through those previous works, the author has found that a pair of vortices can be produced when the fluid passes by the inclined rod and plate. In this way, the longitudinal swirl flow can be generated. Thus, a novel insert is designed and detailed illustrated in the local magnified picture in Fig. 9. The ellipse-shaped inner structure is used to disturb the fluid and generate longitudinal flow and two ends of the inclined vortex plate are mounted on the absorber plate and bottom respectively. As for grid system in simulation, the grid near the inserts is also extremely dense, which always guarantees $y^+ \approx 1$ so that the total grids is over 11 million. The generated streamlines which visualizes the flow are depicted in Fig. 9 for Re = 12,000. Obviously, when the fluid flows through the duct, the streamlines are bent by the guide of inclined vortex plate periodically, which indicates a strong perturbation of the fluid in the whole test section.

In Fig. 10, the inspection of velocity and temperature distribution has been conducted in the plane of x = 0.8 m at Re = 12,000. It is apparent that each inclined vortex plate produces a pair counter-rotating vortices. Therefore, while flowing forward, the fluid in the duct periodically flows from the core region to the wall, and then flows from the boundary region to the core region so as to form longitudinal swirls. With further analyses, it can be deduced that no backflow occurs so that the resistance does not increase much in this way. The results of the above analyses agree well with the design ideas. Thus, the inclined plate can be applied to solve the problem of longitudinal swirl flow realization.

In addition, for the duct fitted with inclined vortex plates, some important numerical results are listed in Table 1. Definitely, the heat transfer and fluid flow characteristics can be improved with the optimization of structure parameters and arrangements. The

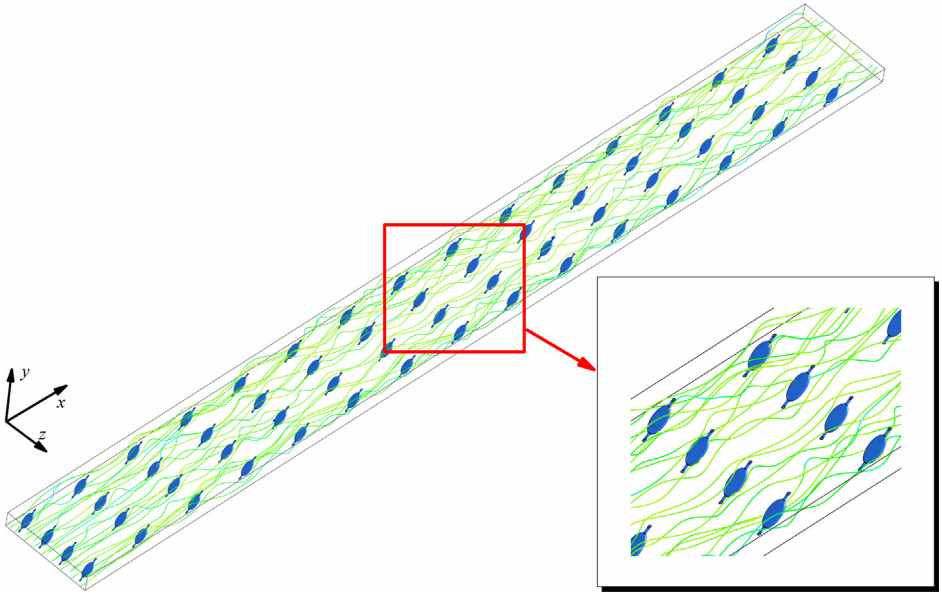

Fig. 9. Streamlines in the duct fitted with inclined vortex plates at Re = 12,000.

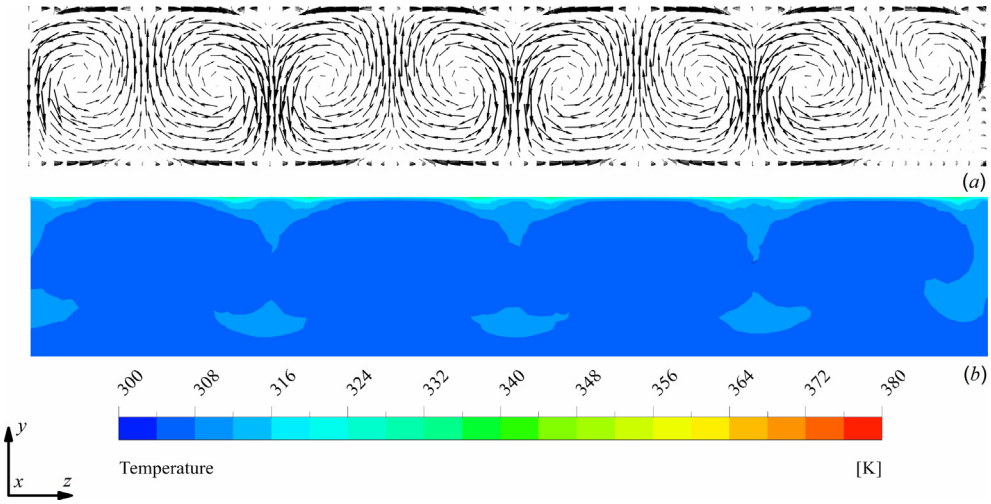

Fig. 10. Tangential velocity distribution and temperature contour in the duct mounted with inclined vortex plates.

Table 1
Numerical results of the duct with inclined vortex plate at Re = 12,000.

Nu/Nu_0	f/f_0	β_m	θ_m	PEC	EEC	T_w	u_r/u_m
2.46	4.92	89.49°	86.97°	1.45	0.5	326 K	0.72

vortex plate location and the distance between two plates can be both adjusted, and structure parameters such as slant angle and plate width can be also optimized. The optimized structure parameters and arrangements can be obtained with genetic algorithm [43]. However, the aim of this part is only the flow pattern realization of longitudinal swirl flow. The further optimization work of this kind of inserts needs the joint efforts of researchers.

7. Conclusion

This paper conducts an approach for optimizing the thermal-hydraulic performance of solar air heater in turbulent flow in order to find the optimized flow pattern. With using the variation method, governing equations are derived when total exergy destruction reaches the minimization point in the heat transfer and fluid flow process. The optimized flow field is obtained by solving the derived governing equations with the SST k–ω turbulent model. With analyses of results, this paper allows following points:

(a) Longitudinal swirl flow is an effective flow pattern for enhancing heat transfer with moderate resistance. With the increase of pump power consumption, the key region where extra heat transfer enhancement measures are urgently needed is varied from boundary flow region to core flow region and then back to boundary flow region.
(b) Heat transfer performance is improved as total heat transfer exergy destruction decreases. In the meanwhile, total exergy destruction of fluid flow and fluid resistance are both increased.
(c) Within the scope of this research, the total heat transfer exergy destruction and average absorber temperature can be maximally reduced by about 65% and 30 K respectively compared with plain duct. Besides, the maximum Nusselt number and friction factor are increased to 1.81 and 3.13 times over plain duct respectively.
(d) A pair of vortices can be produced after the fluid passes by the inclined rod and plate. Thus, the inclined plate can be applied to realize the longitudinal swirl flow.

The future work is to optimize structure parameters and arrangements of the proposed inclined plates in solar air heaters so that the overall thermal-hydraulic performance can be improved. Furthermore, it needs the effort of researchers to conceive of novel structures to realize the obtained optimized flow pattern.

Conflict of interest

There are no known conflicts of interest associated with this publication.

Acknowledgement

This work was supported by the National Natural Science Foundation of China (No. 51736004 and No. 51776079).

References

[1] A.E. Kabeel, M.H. Hamed, Z.M. Omara, A.W. Kandeal, Solar air heaters: design configurations, improvement methods and applications – a detailed review, Renew. Sustain. Energy Rev. 70 (2017) 1189–1206.
[2] F. Wang, Z. Cheng, J. Tan, Y. Yuan, Y. Shuai, L. Liu, Progress in concentrated solar power technology with parabolic trough collector system: a comprehensive review, Renew. Sustain. Energy Rev. 79 (2017) 1314–1328.
[3] X. Chen, F. Wang, Y. Han, R. Yu, Z. Cheng, Thermochemical storage analysis of the dry reforming of methane in foam solar reactor, Energy Convers. Manage. 158 (2018) 489–498.
[4] D. Alta, E. Bilgili, C. Ertekin, O. Yaldiz, Experimental investigation of three different solar air heaters: energy and exergy analyses, Appl. Energy 87 (10) (2010) 2953–2973.
[5] M. Yang, X. Yang, X. Li, Z. Wang, P. Wang, Design and optimization of a solar air heater with offset strip fin absorber plate, Appl. Energy 113 (2014) 1349–1362.
[6] W. Gao, W. Lin, T. Liu, C. Xia, Analytical and experimental studies on the thermal performance of cross-corrugated and flat-plate solar air heaters, Appl. Energy 84 (4) (2007) 425–441.
[7] T. Alam, M.H. Kim, A critical review on artificial roughness provided in rectangular solar air heater duct, Renew. Sustain. Energy Rev. 69 (2017) 387–400.
[8] A. Kumar, M.H. Kim, Heat transfer and fluid flow characteristics in air duct with various V-pattern rib roughness on the heated plate: a comparative study, Energy 103 (2016) 75–85.

[9] B. Bhushan, R. Singh, Nusselt number and friction factor correlations for solar air heater duct having artificially roughened absorber plate, Sol. Energy 85 (5) (2011) 1109–1118.
[10] A. Kumar, R.P. Saini, J.S. Saini, Experimental investigation on heat transfer and fluid flow characteristics of air flow in a rectangular duct with Multi v-shaped rib with gap roughness on the heated plate, Sol. Energy 86 (6) (2012) 1733–1749.
[11] D. Jin, J. Zuo, S. Quan, S. Xu, H. Gao, Thermohydraulic performance of solar air heater with staggered multiple V-shaped ribs on the absorber plate, Energy 127 (2017) 68–77.
[12] A.S. Yadav, J.L. Bhagoria, A CFD based thermo-hydraulic performance analysis of an artificially roughened solar air heater having equilateral triangular sectioned rib roughness on the absorber plate, Int. J. Heat Mass Transf. 70 (2014) 1016–1039.
[13] M.S. Manjunath, K.V. Karanth, N.Y. Sharma, Numerical analysis of the influence of spherical turbulence generators on heat transfer enhancement of flat plate solar air heater, Energy 121 (2017) 616–630.
[14] F. Menasria, M. Zedairia, A. Moummi, Numerical study of thermohydraulic performance of solar air heater duct equipped with novel continuous rectangular baffles with high aspect ratio, Energy 133 (2017) 593–608.
[15] M.M. Alkilani, K. Sopian, M.A. Alghoul, M. Sohif, M.H. Ruslan, Review of solar air collectors with thermal storage units, Renew. Sustain. Energy Rev. 15 (3) (2011) 1476–1490.
[16] W. Chien, Variational principles and generalized variational principles in hydrodynamics of viscous fluids, Appl. Math. Mech. 5 (3) (1984) 1281–1296.
[17] J.A. Meng, X.G. Liang, Z.X. Li, Field synergy optimization and enhanced heat transfer by multi-longitudinal vortexes flow in tube, Int. J. Heat Mass Transf. 48 (16) (2005) 3331–3337.
[18] Q. Chen, M. Wang, N. Pan, Z. Guo, Optimization principles for convective heat transfer, Energy 34 (9) (2009) 1199–1206.
[19] W. Liu, H. Jia, Z.C. Liu, H.S. Fang, K. Yang, The approach of minimum heat consumption and its applications in convective heat transfer optimization, Int. J. Heat Mass Transf. 57 (1) (2013) 389–396.
[20] K. Guo, B. Liu, X. Li, H. Liu, C. Liu, Flow pattern construction-based tubular heat transfer intensification using calculus of variations, Chem. Eng. Sci. 152 (2016) 568–578.
[21] J. Wang, W. Liu, Z.C. Liu, The application of exergy destruction minimization in convective heat transfer optimization, Appl. Therm. Eng. 88 (2015) 384–390.
[22] W. Liu, P. Liu, J.B. Wang, N.B. Zheng, Z.C. Liu, Exergy destruction minimization: a principle to convective heat transfer enhancement, Int. J. Heat Mass Transf. 122 (2018) 11–21.
[23] P. Liu, N. Zheng, F. Shan, Z.C. Liu, W. Liu, Numerical study on characteristics of heat transfer and friction factor in a circular tube with central slant rods, Int. J. Heat Mass Transf. 99 (2016) 268–282.
[24] N. Zheng, P. Liu, F. Shan, Z.C. Liu, W. Liu, Effects of rib arrangements on the flow pattern and heat transfer in an internally ribbed heat exchanger tube, Int. J. Therm. Sci. 101 (2016) 93–105.
[25] P. Liu, N. Zheng, F. Shan, Z.C. Liu, W. Liu, An experimental and numerical study on the laminar heat transfer and flow characteristics of a circular tube fitted with multiple conical strips inserts, Int. J. Heat Mass Transf. 117 (2018) 691–709.
[26] Y. Liu, Q. Chen, K. Hu, J. Hao, Porosity distribution optimization catalyst for methanol decomposition in solar parabolic trough receiver-reactors by the variational method, Appl. Therm. Eng. 129 (2018) 1563–1572.
[27] S.A. Kalogirou, S. Karellas, K. Braimakis, C. Stanciu, V. Badescu, Exergy analysis of solar thermal collectors and processes, Prog. Energy Combust. Sci. 56 (2016) 106–137.
[28] M. Abuşka, Energy and exergy analysis of solar air heater having new design absorber plate with conical surface, Appl. Therm. Eng. 131 (2018) 115–124.
[29] F. Bayrak, H.F. Oztop, A. Hepbasli, Energy and exergy analyses of porous baffles inserted solar air heaters for building applications, Energy Build. 57 (2013) 338–345.
[30] American Society of Heating. Refrigeration and Air Conditioning Engineers (ASHRAE) Standard 93-2003, Atlanta, 2003.
[31] A. Kumar, M.H. Kim, Effect of roughness width ratios in discrete multi V-rib with staggered rib roughness on overall thermal performance of solar air channel, Sol. Energy 119 (2015) 399–414.
[32] Y.L. He, W.Q. Tao, Chapter three – convective heat transfer enhancement: mechanisms, techniques, and performance evaluation, in: E.M. Sparrow, J. Abraham, J. Gorman, Y. Cho (Eds.), Advances in Heat Transfer, Elsevier, 2014, pp. 87–186.
[33] W. Liu, P. Liu, Z.M. Dong, K. Yang, Z.C. Liu, A study on the multi-field synergy principle of convective heat and mass transfer enhancement, Int. J. Heat Mass Transf. 134 (2019) 722–734.
[34] W. Liu, J.B. Wang, Z.C. Liu, A method of fluid dynamic analysis based on Navier-Stokes equation and conservation equation on fluid mechanical energy, Int. J. Heat Mass Transf. 109 (2017) 393–396.
[35] R. Webb, Performance evaluation criteria for use of enhanced heat transfer surfaces in heat exchanger design, Int. J. Heat Mass Transf. 24 (4) (1981) 715–726.
[36] A. Bejan, Entropy generation through heat and fluid flow, Wiley, 1982.
[37] W. Liu, Z.C. Liu, L. Ma, Application of a multi-field synergy principle in the performance evaluation of convective heat transfer enhancement in a tube, Chin. Sci. Bull. 57 (13) (2012) 1600–1607.
[38] H. Xiao, J. Wang, Z.C. Liu, W. Liu, A consistent SIMPLE algorithm with extra explicit prediction — SIMPLEPC, Int. J. Heat Mass Transf. 120 (2018) 1255–1265.
[39] S.V. Patankar, Numerical HeatTransfer and Fluid Flow, Hemisphere, Washington D.C., 1980.
[40] V.B. Gawande, A.S. Dhoble, D.B. Zodpe, S. Chamoli, A review of CFD methodology used in literature for predicting thermo-hydraulic performance of a roughened solar air heater, Renew. Sustain. Energy Rev. 54 (2016) 550–605.
[41] E.A. Handoyo, D. Ichsani Prabowo, Sutardi, Numerical studies on the effect of delta-shaped obstacles' spacing on the heat transfer and pressure drop in v-corrugated channel of solar air heater, Sol. Energy 131 (2016) 47–60.
[42] F.R. Menter, Review of the shear-stress transport turbulence model experience from an industrial perspective, Int. J. Comput. Fluid Dyn. 23 (4) (2009) 305–316.
[43] Z.C. Liu, S. Zhu, Y. Ge, F. Shan, L. Zeng, W. Liu, Geometry optimization of two-stage thermoelectric generators using simplified conjugate-gradient method, Appl. Energy 190 (2017) 540–552.